Fast Electromigration Immortality Analysis for Multisegment Copper Interconnect Wires

Zeyu Sun, *Student Member, IEEE*, Ertugrul Demircan, *Senior Member, IEEE*, Mehul D. Shroff, Chase Cook, *Student Member, IEEE*, and Sheldon X.-D. Tan, *Senior Member, IEEE*

***Abstract*—In this paper, we present a novel and fast electromigration (EM) immortality check for general multisegment interconnect wires. Instead of using current density as the key parameter, as in traditional EM analysis methods based on Black's equation and the Blech limit, the new method estimates the EM-induced steady-state stress in general multisegment copper interconnect wires based on a novel parameter, *Critical EM Voltage,* $V_{\mathrm{Crit,EM}}$. We show that the $V_{\mathrm{Crit,EM}}$ is essentially the natural, but important, extension of the *Blech limit* concept, which describes the EM immortality condition for a single segment wire, to more general multisegment interconnect wires. The proposed method, called voltage-based EM (VBEM) method, mitigates the problem of current-density-based EM criteria, which can only be applied to a single wire. The new VBEM method can naturally comprehend the impact of the topology of the wire structure on EM-induced stress. As a result, this new VBEM analysis method is very amenable to addressing EM violations, as it brings new optimization capabilities to the physical design flow. The VBEM stress estimation method is based on the fundamental steady-state stress equations. This approach avoids computationally intensive numerical methods and can be implemented in CAD tools very easily, as we demonstrate on real design examples. We also show that the proposed VBEM analysis method agrees with results from the finite difference method in the steady state through one example and also agrees with one published closed-form expression of steady-state stress for a special 3-terminal wire case. Furthermore, we compare VBEM against the COMSOL finite element analysis tool and another published EM numerical simulator XSim, validated by measured results, which shows that VBEM agrees with both of them very well in terms of accuracy and thus further validates the proposed method. We also study the impact of current crowding in practical interconnect wires on the estimated steady-state stress, which are shown to be not significant if the length of the wire is much greater than its width. An extension of the VBEM method to consider the significant current crowding effects is also shown and additionally, we analyze mesh-structured interconnect wires and demonstrate that the proposed VBEM method is correct and accurate on such structures.**

***Index Terms*—Integrated circuit interconnections, integrated circuit reliability.**

I. Introduction

RELIABILITY has become a major design challenge and limiting factor for nanometer very large scale integration (VLSI) designs. As VLSI technology features are pushed to the limit with each successive generation and with the introduction of new materials and increased current densities to satisfy performance demands, electromigration (EM) is projected to be a key reliability issue for current and future VLSI technologies. It has been predicted that EM failure will become more significant for interconnects in FinFET-based technologies at 10 nm and beyond due to increased current density and elevated heating. Traditional compact EM checking approaches such as Black's equation [1] and Blech product [2] can lead to significant over-design [3]. These conservative design rules are not suitable for future technology scaling since more design guard bands are required for chip timing accuracy, and thus such a worst-case design methodology results in inefficiency and considerable penalties in area, performance, power, and reliability budgets. Existing EM signoff mainly relies on current density-based assessment using the very conservative Black's model. Such a model does not work well for multisegment interconnect wires as the stresses developed in each wire segment are not independent of one another, which means that although some or all segments may be EM-immortal, the whole tree wire can still be EM-mortal [4], [5]. An interconnect tree wire is defined as continuously connected metal (copper or aluminum) within one layer of metallization. These trees terminate at diffusion barriers at vias and contacts and can have more than one terminating segment, as shown in Fig. 1. Existing EM modeling and analysis techniques mainly focus on the simple straight line interconnect with two line-end terminals. However, a practical integrated circuit layout often has interconnects such as clock and power grid networks containing many such interconnect tree wires. The EM effects in the segments of a wire are not independent and they have to be considered simultaneously. As a result, more accurate EM modeling and lifetime analysis approaches are required for complicated interconnect tree wires.

Manuscript received May 10, 2017; revised August 11, 2017 and November 26, 2017; accepted January 10, 2018. Date of publication February 2, 2018; date of current version November 20, 2018. This work was supported in part by the NSF under Grant CCF-1527324, and in part by the DARPA under Grant HR0011-16-2-0009. This paper was recommended by Associate Editor Y. Cao. *(Corresponding author: Sheldon X.-D. Tan.)*

Z. Sun, C. Cook, and S. X.-D. Tan are with the Department of Electrical and Computer Engineering, University of California at Riverside, Riverside, CA 92521 USA (e-mail: sheldon.tan@ucr.edu).

E. Demircan is with the Physical Verification Group, NXP Semiconductors, Austin, TX 78735 USA.

M. D. Shroff is with the Intrinsic Reliability Group, NXP Semiconductors, Austin, TX 78735 USA.

Color versions of one or more of the figures in this paper are available online at http://ieeexplore.ieee.org.

Digital Object Identifier 10.1109/TCAD.2018.2801221

0278-0070 © 2018 IEEE. Personal use is permitted, but republication/redistribution requires IEEE permission.
See http://www.ieee.org/publications_standards/publications/rights/index.html for more information.

Authorized licensed use limited to: Univ of Calif Riverside. Downloaded on June 24,2026 at 00:38:02 UTC from IEEE Xplore. Restrictions apply.

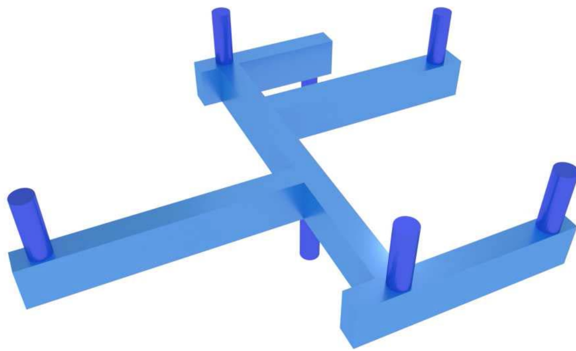

Fig. 1. Interconnect tree confined by diffusion barriers/liners.

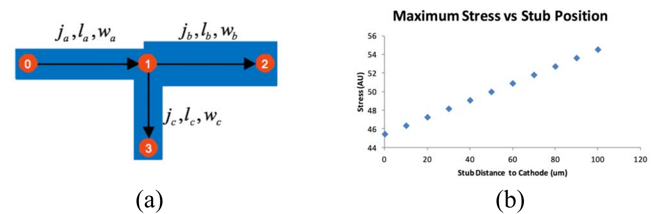

(a) (b)

Fig. 2. (a) Illustration of T-junction interconnect with directed graph inserted to indicate electron flow. (b) Stress at the cathode end increases linearly as the stub is placed further away from the cathode end.

Currently, employed approaches that use the Blech length [2] (for the elimination of immortal segments) and Black's equation [1] are based on measurements from single wires. They ignore the geometry and topology impacts on the EM failure effects. To mitigate this problem, the *effective line length and current density product*, $(jL)_{\text{eff}}$ was proposed [4], [5], which takes into account the maximum of summation of all the possible Blech products from any two nodes in a tree. However, such individual-branch-based approaches lack theoretical support and can lead to over-estimation as the $(jL)_{\text{eff}}$ may reach the given threshold, but the maximum stress in the wires can still be less than that critical stress [6].

In order to avoid these problems, some physics-based EM analysis methods, based on solving the basic mass transport equation for through-silicon via (TSV) and power grid networks, have recently been proposed [7]–[10]. These models address the resistance changes of a wire over time as the atomic concentration changes due to atomic flux. Since these proposed methods solve the basic mass transport equations using the finite element method, which is computationally expensive, they can only solve for very small structures such as one TSV structure. Complicated look-up tables or models have to be built for different TSVs and wire segments for full-chip power grid analysis at reduced accuracy.

Alternatively, a more compact physics-based EM model [11], based on the solution of the hydrostatic stress distribution equation [12], has been proposed. This model is derived from a single wire. It can consider many geometry parameters like wire lengths, residual stress, etc. This model has also been extended to consider the multi-branch interconnects based on the projected steady-state stress. However, complicated equations have to be solved based on the current density of each branch. Recently, a compact EM model which can provide the time-dependent evolution of the hydrostatic stress for multibranch interconnect wires has been proposed [13]. However, this model can only deal with a limited number of interconnect structures and cannot deal with general interconnect topologies. An integral transformation-based method was proposed recently to obtain the analytic solution for multisegment wires in straight lines [14]. However, this method needs many terms (a few hundred) to obtain accurate results and was mainly for transient stress analysis. Recently, a more general finite difference time domain-based numerical analysis method has been proposed to solve the stress partial differential equations (PDEs) [15], [16]. Still, these methods are still computationally intensive for full-chip level analysis.

Recently, work in [6] proposed a method for checking the EM immortality of multisegment interconnect tree. The method is based on the atomic concentrations and its relationship with the stress in the steady-state to derive the stress conservation equation. This method can compute the steady state for each branch (their terminal nodes) so that EM immortality is checked for each branch.[1] However, this method is still different from the voltage-based EM (VBEM) method in the following aspects: first, this method still focuses on the individual branch for checking EM immortality and no global EM immortality check criteria were proposed for the whole interconnect tree. Second, no closed-form expressions were proposed to compute the steady-state stress for each node in the interconnect tree.

To further illustrate wire topology impacts on the EM-induced stress, Fig. 2 shows a T-shaped wire with branch 3 as a stub. If one changes the stub location of the wires as shown in Fig. 2(a), [branch (1,3) is a stub if current density on that branch $j_c = 0$], the projected steady-state stress (the maximum stress the wire can reach in steady-state) will change noticeably as shown in Fig. 2(b). As one can see, the location of the stub in the wire can change steady-state stress at the cathode node significantly.

In this paper, we present a novel and fast EM immortality check for general multisegment interconnect wires. Different from the traditional *Blech product*-based method, which focuses on single wires using current density, the new method estimates the EM-induced steady-state stress in general multisegment copper interconnect wires based on a novel parameter, *Critical EM Voltage*, or $V_{\text{Crit,EM}}$. We show that the $V_{\text{Crit,EM}}$ essentially is the natural, but important extension of the *Blech product* or *Blech limit* concept, which describes the EM immortality condition for a single segment wire, to more general multisegment interconnect wires. The new method estimates the EM-induced steady-state stress of general multisegment interconnect wires based on the terminal voltages or

[1]We realized that (14) in [6] is indeed almost identical to (8). However, we would like to mention that the two methods were developed independently. Actually the original idea of the proposed work was first proposed in [17], which was published in 2014 and was extended in [18], while the work in [6] was published in 2015.

Authorized licensed use limited to: Univ of Calif Riverside. Downloaded on June 24,2026 at 00:38:02 UTC from IEEE Xplore. Restrictions apply.

potentials of the wire. Specifically, our new contributions are summarized below.

1) We propose a new EM failure criterion called $V_{\mathrm{Crit,EM}}$, which can be viewed as the extended *Blech product* or *Blech limit* for multisegment interconnect wires for fast detection of EM immortality of those wires. It mitigates the problem of current-density-based EM criteria, which can be applied to a single wire. It can become a new foundry parameter for guiding the EM-aware physical design and EM signoff analysis.
2) We show that the proposed VBEM assessment technique can naturally comprehend the impact of the topology of the wire structure on EM-induced stress as it does not consider the branch related information such as branch currents anymore. This new VBEM analysis method is very amenable for addressing EM violations as it brings new design capabilities into the physical design flow. The new VBEM stress estimation method is based on the fundamental steady-state stress equations.
3) We show that the proposed VBEM analysis method agrees with the results from the finite difference method in the steady state through one example, which validates the proposed VBEM analysis method.
4) We also show that the VBEM result agrees with one published closed-form expression of steady-state stress for a special 3-terminal wire case. The published expression is consistent with the measured results.
5) We compare the VBEM method against the COMSOL finite element analysis (FEA) tool and another published EM numerical simulator XSim [19], which has been validated by measured results [19], [20] and we show that VBEM agrees with both of them very well for steady state stress in terms of accuracy.
6) We also study the impact of current crowding effects of practical interconnect wires on the estimated steady-state stress by the VBEM method. This paper shows that if all the wire segments are long enough (compared to the wire width), the current crowding impacts on EM values as determined by the VBEM method are not significant.
7) Furthermore, we analyze mesh-structured interconnect wires and demonstrate that the proposed VBEM method is correct and accurate on these structures. Our results show that the VBEM method leads to less than 0.17% error compared to COMSOL for all the cases, which shows that the proposed VBEM method can be directly applied to mesh-structured wires.

This approach avoids the computationally intensive numerical approaches to obtain the steady-state stress for complicated interconnects and can be implemented in CAD tools very easily as we demonstrate on real design examples. Our experimental results show that the new method is consistent with the physics-based dynamic EM stress evaluations from the numerical analysis by COMSOL.

This paper is organized as follows. Section II reviews the basic EM physics and existing EM-induced stress evolution modeling at the steady state and in the time domain. Section III presents the new voltage-based steady-state EM-induced stress analysis and the concept of the $V_{\mathrm{Crit,EM}}$. We demonstrate the proposed method through several practical examples and discuss the impact of current crowding and application of the new method to the mesh-structured multisegment interconnect wires. Section IV presents some numerical results and comparison against the finite element-based COMSOL. Section V concludes this paper.

II. EM Physics and Stress Modeling

EM is a physical phenomenon of the migration of metal atoms along the direction of the applied electrical field. Atoms (either lattice atoms or defects/impurities) migrate toward the anode end of metal wire along the trajectory of conducting electrons. During the migration process, hydrostatic stress generated inside the confined metal wire due to momentum exchange between lattice atoms and conducting electrons is a prime cause of void and hillock formation at the opposite ends of the wire. Indeed, when a metal wire is embedded into a rigid confinement, which is the case with copper interconnect metallization, the wire volume changes (induced by the atom depletion and accumulation due to migration) create tension at the cathode end and compression at the anode ends of the line. Over time, the lasting unidirectional electrical load will increase hydrostatic stress, as well as the stress gradient which acts as a counter-force for atomic migration along the metal line. In some cases, usually, when a line is long, this stress can reach a critical level, resulting in void nucleation at the cathode end and/or hillock formation at the anode end of line.

Specifically, let $\sigma(x)$ denote the stress at location x, the atomic flux, Γ_σ, caused by the inhomogeneous distribution of the hydrostatic stress is [12]

$$\Gamma_\sigma = \frac{D_a}{kT}\frac{\partial \sigma}{\partial x}. \tag{1}$$

The atomic flux flowing toward the anode caused by EM effects, Γ_{EM}, can be described by

$$\Gamma_{\mathrm{EM}} = \frac{D_a}{\Omega kT} eZ\rho j \tag{2}$$

where $D_a = D_0\exp(E_a/kT)$ is the effective atomic diffusivity, E_a is the activation energy of the failure process, T is the absolute temperature and k is the Boltzmann constant. Ω is the atomic lattice volume, e is the electron charge, eZ is the effective charge of the migrating atoms, ρ is the wire electrical resistivity, and j is current density.

A. Steady-State EM-Induced Stress Modeling

At the steady state, the atomic flux becomes zero, which means that $\Gamma_\sigma = \Gamma_{\mathrm{EM}}$. As a result, we have

$$\frac{\partial \sigma}{\partial x} = \frac{eZ\rho}{\Omega} j. \tag{3}$$

On the other hand, the hydrostatic stress also leads to displacement of interconnect materials, which can be described as

$$\frac{\partial u}{\partial x} = \alpha\sigma \tag{4}$$

$$\sum_k u_{ik} w_{ik} = 0 \tag{5}$$

Authorized licensed use limited to: Univ of Calif Riverside. Downloaded on June 24,2026 at 00:38:02 UTC from IEEE Xplore. Restrictions apply.

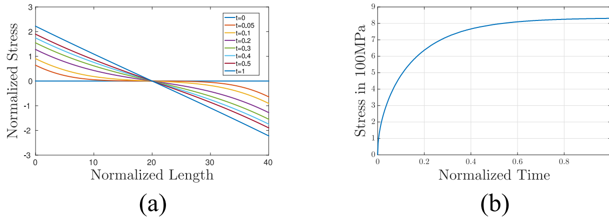

Fig. 3. (a) EM-stress distribution change over time in a simple metal wire. (b) EM-stress evolution versus time.

where, u_{ik} is the displacement and w_{ik} is the width at the kth node on a branch between nodes i and k, and $M = 1/\alpha$ is the Young's modulus of the interconnect materials [17].

We note that (4) and (5) can be viewed as the atomic conservation (in the sense that the total number of metal atoms will remain the same during the migration process in the wire) in the stress kinetics. We notice that a similar conservation equation was given in [11] for steady-state stress computation for multibranch interconnects.

B. Transient EM-Induced Stress Modeling

More complete modeling of transient hydrostatic stress evolution due to EM effects was proposed by Korhonen [12]. In this model, for a wire segment with length L, stress $\sigma(x, t)$ in the 1-D case can be described by Korhonen's PDE with copper migration-blocking boundary condition (BC)

$$\begin{aligned} \text{PDE}: \frac{\partial \sigma}{\partial t} &= \frac{\partial}{\partial x}\left[\kappa\left(\frac{\partial \sigma}{\partial x} + G\right)\right] \\ \text{BC}: \frac{\partial \sigma}{\partial x}(0, t) &= G,\ \frac{\partial \sigma}{\partial x}(L, t) = -G \end{aligned} \tag{6}$$

where, $\kappa = D_a B\Omega/kT$, B is the effective bulk elasticity modulus, Ω is the atomic lattice volume, $G = (eZ\rho j/\Omega)$ is the EM driving force, where e is the electron charge, eZ is the effective charge of the migrating atoms, ρ is the wire electrical resistivity, and j is the current density. Existing physics-based models are mainly based on the solutions of Korhonen's equation [11], [13], [21].

Fig. 3(a) shows stress development over time in a metal line with Korhonen's equation. Over time, tensile (positive) stress will be developed at the cathode node (left) and compressive (negative) stress will be developed at the anode node (right). The stress changes polarity in the middle of the wire. The built-up stress (its gradient) will serve as the counter-force for atomic flux. Fig. 3(b) shows stress evolution at the cathode, which reaches a steady state over time. If the highest stress at the cathode node exceeds the critical stress, then voids will be created and will start to grow until they reach critical sizes (which depends on the via/wire structures and current flow direction) and resistance starts to increase, which may eventually lead to the resistance becoming unacceptably high or even causing catastrophic failures due to formation of an open circuit. However, in this paper, we primarily focus on whether a void will form or not in the first place.

Fig. 4. Three-terminal wire, with the direction indicating electron flow.

III. Voltage-Based EM Stress Estimation

In this section, we first present the compact EM model based on the solution of steady-state modeling of EM effects, which lead to the voltage-based assessment for EM failures for interconnect trees. We then show that the VBEM assessment is more suitable for multibranch interconnect trees. We compare the results from the voltage-based VBEM with results from dynamic EM models to validate the new VBEM model on some complex interconnect wire structures.

A. New Voltage-Based Analysis for Steady-State EM Stress

One important observation is that the stress difference between two nodes at the steady state can be expressed in terms of voltage, instead of current density [17]. To demonstrate this, suppose that we have N nodes in the interconnect tree. We can discretize (3) in space, if we ignore the initial or residual stress, leading to

$$\sigma_k - \sigma_i = \frac{eZ\rho}{\Omega} l_{ik} j = \frac{eZ}{\Omega} V_{ik} \tag{7}$$

where σ_k is the steady-state stress at node k, and V_{ik} is the voltage or potential difference from node i and node k. When $V_{ik} > 0$, stress at node k is higher than the stress at node i (we assume that tensile stress is positive and compressive stress is negative).

From (4) and (5), we have

$$\sum_{k}^{N} a_k \sigma_k = 0 \tag{8}$$

where a_k is the total area of the branches connected to the node k. This equation represents the conservation in the stress kinetics. Note that (8) does not include the initial residual stress as we will consider that later. For instance, in Fig. 4, the area for node 1 is $l_a w_a + l_b w_b$. For this case, (8) can be expressed as $l_a w_a \sigma_0 + (l_a w_a + l_b w_b)\sigma_1 + l_b w_b \sigma_2 = 0$. We also notice that for this case, we have

$$\sum_{k}^{N} a_k = l_a w_a + l_a w_a + l_b w_b + l_b w_b = 2(l_a w_a + l_b w_b) = 2A \tag{9}$$

where A is the total area of the branches in the wire. By considering (7), we can compute the stress for any node i in terms of all the node voltages with respect to the node i

$$\sigma_i = \frac{\beta}{2A} \sum_{k \neq i}^{N} a_k V_k^i \tag{10}$$

where $\beta = (eZ/\Omega)$, and V_k^i is the nodal voltage at node k with respect to node i (node i is treated as the reference node).

Authorized licensed use limited to: Univ of Calif Riverside. Downloaded on June 24,2026 at 00:38:02 UTC from IEEE Xplore. Restrictions apply.

If we select the reference node as the ground node with the lowest voltage of the segment, then the stress at this node can be expressed as

$$\sigma_g = \frac{\beta}{2A}\sum_{k\neq g}^{N} a_k V_k \tag{11}$$

where, V_k is the normal nodal voltage (with respect to cathode node g) at the node k in the wire. The cathode node is where the tensile stress σ_g is the highest in the segment.

If we further define a virtual voltage as

$$V_E = \frac{1}{2A}\sum_{k\neq g}^{N} a_k V_k \tag{12}$$

which can be viewed as *EM Voltage*, then according to (7), the stress at any node with nodal voltage V_i (with respect to ground node), can then be computed easily as in [17].

Furthermore, if the current density is not evenly distributed, an integration is required to calculate the *EM voltage* as follows:

$$V_E = \frac{1}{A}\iint V(x,y)dxdy. \tag{13}$$

Then the steady-state stress at the node i can be calculated as

$$\sigma_i \ = \beta(V_E - V_i). \tag{14}$$

This equation shows that the EM-induced stress at any node can be easily determined by the difference between the node voltage and the *EM voltage* for an interconnect segment. Therefore, EM stress determination is simplified to a problem of analyzing the node potentials and combining them with geometric information of the interconnect. Node potentials are readily available after circuit simulation and additional numerical computation is not required.

For EM effects, when the hydrostatic stress (EM-induced stress plus other existing stresses) at a node hits the critical stress, σ_{crit}, then the void starts to be nucleated and the resistance of the wire starts to increase over time, which can be measured experimentally [22], [23].

Assuming that initial or residual stress is σ_{init}, which is the same for all the nodes (this may not be true in general, but we have used the assumption to simplify our presentation), then we can determine the voltage required for the nucleation to happen called $V_{\text{Crit,EM}}$ defined as

$$V_{\text{crit,EM}} = \frac{\Omega}{Ze}(\sigma_{\text{crit}} - \sigma_{\text{init}}). \tag{15}$$

The significance of $V_{\text{Crit,EM}}$ is that it essentially is the natural, but important extension of *Blech product* or *Blech limit* concept, which describes the EM immortality condition for a single-segment wire, to more general multisegment interconnect wires (we will discuss this more in the next section). Specifically, for any nodal voltage V_i, one only needs to further check whether

$$V_{\text{Crit,EM}} > V_E - V_i. \tag{16}$$

If this condition is met for all the terminal voltages of the wire, then no EM failures will happen. Typically, for a multibranch wire, when it is stressed only by positive voltages, if $V_E < V_{\text{Crit,EM}}$, no wire will have an EM failure because even the cathode node (with the lowest voltage) will not fail in this case. Otherwise, EM failures may happen. This makes the immortality check much more efficient as we typically only need to check one node for an interconnect segment, instead of checking every branch as is done for the traditional method. Note that if we have multiple nodes failing (16), all those nodes can lead to nucleation. However, for the question of EM immortality, as long as one node fails as per (16), the whole tree is mortal.

On the other hand, if a wire fails the immortality check in (16), then more detailed and time-dependent stress analysis is required to determine the time-to-failure or mean time-to-failure, which still remains a difficult problem for general multibranch interconnect trees [13].

B. General and Key VBEM Equations

In this section, we summarize the general and key VBEM equations used for the EM immortality check. For a given arbitrary interconnect tree with N nodes, assuming the voltage in node i is V_i and the ground node is g and $V_g = 0$, then the stress at the node i can be computed as

$$\sigma_i = \frac{eZ}{\Omega}\left(\frac{1}{2A}\sum_{k\neq g}^{N} a_k V_k - V_i\right). \tag{17}$$

Given the $V_{\text{Crit,EM}}$, then EM immortality check for node i becomes

$$V_{\text{Crit,EM}} > \frac{1}{2A}\sum_{k\neq g}^{N} a_k V_k - V_i. \tag{18}$$

We want to remark that as far as immortality/mortality is concerned, we are only interested in whether or not there exists at least one void formed in a given wire. If no void is formed, the wire is immortal, else the wire is mortal. Hence, we only need to look at the node with lowest voltage, the ground node or cathode node of the whole tree, as a result, (18) can be simplified to

$$V_{\text{Crit,EM}} > \frac{1}{2A}\sum_{k\neq g}^{N} a_k V_k. \tag{19}$$

If (19) fails, then transient EM analysis will be carried out to find the void location and the nucleation time.

C. Relationship to the Blech limit

In this section, we show how our VBEM analysis and $V_{\text{Crit,EM}}$ is related to the existing Blech limit. We first show that the Blech product essentially is the VBEM assessment for just one wire segment. The proposed VBEM method can actually be viewed as the general extension of this technique to multibranch interconnect wires.

Specifically, let L be the length of a single wire and j the current density of the wire. Starting with the steady-state condition of EM stress shown in (3), which is also called the

Authorized licensed use limited to: Univ of Calif Riverside. Downloaded on June 24,2026 at 00:38:02 UTC from IEEE Xplore. Restrictions apply.

Blech condition, if we integrate (3) along the line, we obtain

$$\sigma(x) = \sigma_{\text{init}} + \frac{eZ\rho j}{\Omega} x \tag{20}$$

where, σ_{init} is the residual stress. The maximum tensile stress can be achieved at the cathode end of the wire ($x = L$).

If the critical stress that the wire can withstand is σ_{crit}, we can define the critical product for EM failure as

$$(jL)_{\text{crit}} = \frac{\Omega(\sigma_{\text{crit}} - \sigma_{\text{init}})}{eZ\rho} \tag{21}$$

which is called the *Blech limit* or *Blech product* [2]. A wire is immortal for EM if it satisfies $jL < (jL)_{\text{crit}}$. As a result, the Blech product can help identify all the immortal wires efficiently.

Notice that if ρ is the resistivity, ρLj is actually the voltage across the wire, then (21) becomes

$$(jL)_{\text{crit}} * \rho = V^b_{\text{crit}} = \frac{\Omega(\sigma_{\text{crit}} - \sigma_{\text{init}})}{eZ} \tag{22}$$

where V^b_{crit} is actually the critical voltage for this single wire. As we can see, this equation is the same as (15) for the single wire case. However, we want to stress that the new $V_{\text{Crit,EM}}$ is more general than the Blech limit due to the following reasons: first, the failure criterion is no longer associated with current density and length of a specific wire segment. In other words, the existing Blech product, jL, does not work any more in this case as the jL of individual branch not only depends on the critical stress, but also depends on the wire structures as the stresses in each wire segment are not independent as they affect each other. However, the proposed $V_{\text{Crit,EM}}$ concept can be applied to general interconnect trees with multisegment wires as one single EM immortality criterion. Second, $V_{\text{Crit,EM}}$ still retains the benefits of the Blech limit as the voltage values can be measured directly based on the pass/fail determination of wires from experiments. Third, it agrees with the Blech limit for the single-wire segment case, which essentially validates the proposed method. It has the potential be used as a new design rule parameter between the foundry and design teams to replace or extend the current Blech limit parameter.

D. Steady-State Analysis

In this section, we first show that the proposed VBEM analysis agrees with the results from the steady-state results computed from the finite difference method. Then we show that it agrees with a published closed-form expression for a special case. We demonstrate this using one example, a three-terminal wire as depicted in Fig. 4.

We first compare with the finite difference method. Let the total length be L. The segment lengths l_a and l_b in the three-terminal wire are equal to $(L/2)$. We then use this wire segment length as the spatial step size and use the backward difference method for boundary derivation as shown in [15]. We remark that the matrix derived by the 1-D finite difference method actually is singular. The reason is that the atomic conservation in the stress kinetics is not observed in this case. In order to resolve this problem, (8) is introduced to replace one row in the matrix. The resulting system of the equations for the three-terminal wire case is presented as

$$\begin{bmatrix} 1 & 0 & 0 \\ 0 & 0 & 0 \\ 0 & 0 & 1 \end{bmatrix} \begin{bmatrix} \dot{\sigma_0} \\ \dot{\sigma_1} \\ \dot{\sigma_2} \end{bmatrix} = \frac{\kappa}{(L/2)^2} \begin{bmatrix} -1 & 1 & 0 \\ 1 & 2 & 1 \\ 0 & 1 & -1 \end{bmatrix} \times \begin{bmatrix} \sigma_0 \\ \sigma_1 \\ \sigma_2 \end{bmatrix} + \begin{bmatrix} \frac{2\kappa G_a}{L} \\ 0 \\ -\frac{2\kappa G_b}{L} \end{bmatrix}. \tag{23}$$

Here, G_a and G_b are the EM driving forces corresponding to segments a and b, respectively. We then rewrite these equations into the following format:

$$\begin{aligned} \mathbf{C}\dot{\sigma}(t) &= \mathbf{A}\sigma(t) + \mathbf{B} \\ y(t) &= \mathbf{E}\sigma(t). \end{aligned} \tag{24}$$

In (24), $\mathbf{E} = (1, 0, 0)$, which means we are looking at the steady state of node 0 which is the cathode node. Then, a Laplace transform can be applied and the transfer function can be obtained as

$$F(s) = \mathbf{E}(s\mathbf{C} - \mathbf{A})^{-1}\mathbf{B}. \tag{25}$$

Under step input, which is $(1/s)$ in frequency domain, the final value theorem can be used to obtain the stress at steady state. If $\lim_{t\to\infty} f(t)$ has a finite limit under a step input, the final value theorem for a function under the step input can be expressed as

$$\lim_{t\to\infty} f(t) = \lim_{s\to 0} sF(s)\frac{1}{s} = F(s)|_{s=0} = -\mathbf{E}\mathbf{A}^{-1}\mathbf{B}. \tag{26}$$

We notice that $(-A)^{-1}$ is

$$(-A)^{-1} = \frac{L^2}{4\kappa} \times \frac{1}{4} \begin{bmatrix} 3 & -1 & -1 \\ -1 & -1 & -1 \\ -1 & -1 & 3 \end{bmatrix}. \tag{27}$$

Then, we can obtain the steady-state result of the system

$$\begin{aligned} \sigma_{\text{steady}} = F(s)|_{s=0} &= \left(\frac{3}{4} \times \frac{2\kappa G_a}{L} + \frac{1}{4} \times \frac{2\kappa G_b}{L}\right)\frac{L^2}{4\kappa} \\ &= \frac{(3G_a + G_b)L}{8}. \end{aligned} \tag{28}$$

On the other hand, we can compute steady-state stress at the cathode node (node 0) based on the voltage-based method as

$$\begin{aligned} \sigma_{\text{steady}} &= V_E \times \beta = \frac{A_1 V_1 + A_2 V_2}{2A} \times \beta \\ &= \frac{j_a L\rho + j_a L\rho/2 + j_b L\rho/2}{4} \times \beta = \frac{(3G_a + G_b)L}{8} \end{aligned} \tag{29}$$

where $V_E = [(A_1V_1 + A_2V_2)/2A]$ is the *EM voltage* at the cathode node and $\beta = (eZ/\Omega)$. As we can see, the results from the two methods are identical. This example gives another theoretical validation of the proposed VBEM analysis method, which agrees with the steady-state results from the finite difference method.

Now we show that the discretization schemes (by using different discretization sizes) will not change the steady-state results. Fig. 6 shows stress analysis using the simplified FDM method comparing COMSOL result of Korhonen's equation.

Authorized licensed use limited to: Univ of Calif Riverside. Downloaded on June 24,2026 at 00:38:02 UTC from IEEE Xplore. Restrictions apply.

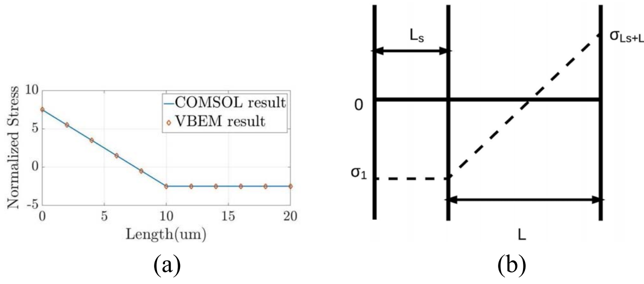

(a) (b)

Fig. 5. (a) 3-terminal wire with inactive (passive) sink, with the cathode at node 2. (b) Steady-state stress distribution of a 3-terminal wire with inactive (passive) sink.

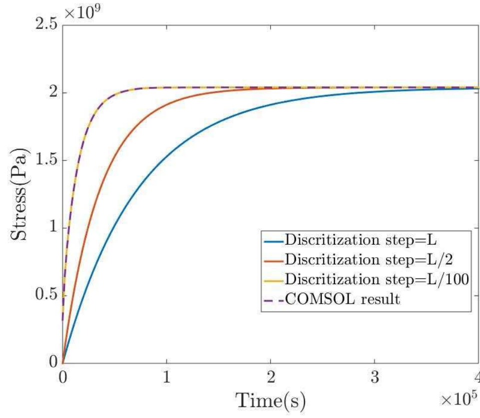

Fig. 6. Different discretization steps (sizes) lead to the same steady-state stress.

It can be observed that the steady-state results under different discretization sizes are same although their transient behaviors are different. In other words, discretization errors will not affect the final steady-state results from FDM.

In addition to analyzing the FDM steady state results considering different discretization schemes, we further show some pole information from the FDM analysis of Korhonen's equation. We use the same 3-terminal wire shown in Fig. 4 as an example. In this case, we discretize the two segments into 21 nodes (so we have 21 poles) instead of just the three boundary nodes presented in (23). As we can see from Table I, all the poles are real poles and the EM system is stable. The EM-induced stress basically is progressing monotonically for a given step current input. Such a monotonic nature of EM-induced stress is important to ensure the steady state is sufficient for the EM immortality check. This paper shows that this is the case for all the examples we analyzed. We also remark that although there is still a possibility of overshoots for a system with negative poles, for our case, it is rarely observed since they are only theoretically possible. Practically, it does not seem necessary to worry about the oscillating behaviors in the stress evolution process.

Furthermore, we notice that recent work in [24] gives the closed-form expression (which is consistent with the measured experimental results) of steady-state stress for a special three-terminal wire case with an inactive (passive) segment [Fig. 5(a)], and the stress profile [Fig. 5(b)]. In this case, the

TABLE I
COMPUTED POLES FOR THE 3-TERMINAL WIRE

Poles values ($\times 10^3$)				
-1.7541	-1.7248	-1.6767	-1.6107	-1.5286
-1.4319	-1.3230	-1.2042	-1.0783	-0.9479
-0.8161	-0.6857	-0.5598	-0.4410	-0.3321
-0.2354	-0.1533	-0.0873	-0.0392	-0.0099
-0.0000	–	–	–	–

segment L_s has zero current (so it is inactive or passive), while the active segment L has current flow j. The cathode is located at node 2. It was shown in [24] that the steady-state stress at any location x in the active segment $\sigma(x)$ is given by

$$\sigma(x) = \frac{e\rho Zj(x - L_s)}{\Omega} + \sigma_1 \tag{30}$$

where σ_1 is the stress in the inactive sink as shown in Fig. 5(b), which is given by

$$\sigma_1 = -\frac{e\rho ZjL^2}{2\Omega(L + L_s)}. \tag{31}$$

As a result, the stress at the cathode node ($x = L_s + L$) will become

$$\begin{aligned}\sigma(L + L_s) &= \frac{e\rho ZjL}{\Omega} - \frac{e\rho ZjL^2}{2\Omega(L + L_s)} \\ &= \frac{e\rho Zj}{\Omega}\left[L - \frac{L^2}{2(L + L_s)}\right].\end{aligned} \tag{32}$$

On the other hand, based on the VBEM method, we have $V_0 = V_1 = jL\rho$ (as there is no current in L_s and $A_0 = L_s w$ and $A_1 = Lw + L_s w$, where w is the width of the two segments (assuming two segments have the same width). Then, the stress at the cathode node, $\sigma(L + L_s)$, can be computed by

$$\begin{aligned}\sigma(L + L_s) &= \beta \times V_E(L + L_s) = \beta \times \frac{A_0 V_0 + A_1 V_1}{2A} \\ &= \beta \times \left[\frac{jL\rho(L_s w + Lw) + jL\rho L_s w}{2(Lw + L_s w)}\right] \\ &= \beta \times \left[\frac{jL\rho}{2} + \frac{jL\rho L_s}{2(L + L_s)}\right] \\ &= \frac{e\rho Zj}{\Omega}\left[L - \frac{L^2}{2(L + L_s)}\right].\end{aligned} \tag{33}$$

Comparing (32) and (33), we can see again that the VBEM method agrees exactly with the closed-form expression for this particular case given by [24].

E. Study of Some Special Cases

In this section, we study three multibranch interconnect structures to illustrate the proposed method. The three structures consist of a straight-line 3-terminal wire in Fig. 7, a T-shaped 4-terminal wire in Fig. 10, and a comb structure wire in Fig. 11. We stress that the proposed method can be applied to any multibranch tree-structured interconnects.

1) Straight-Line 3-Terminal Wire: The straight-line 3-terminal wire is shown in Fig. 7. In this wire, the node 0 is treated as the ground node. Note that current densities in the two segments are j_a and j_b, which are determined by the rest

Authorized licensed use limited to: Univ of Calif Riverside. Downloaded on June 24,2026 at 00:38:02 UTC from IEEE Xplore. Restrictions apply.

Fig. 7. Interconnect examples for EM analysis for a straight-line 3-terminal wire.

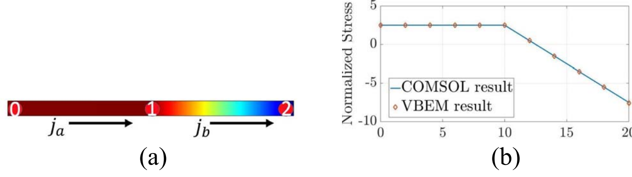

Fig. 8. (a) 2-D stress distribution on wire at steady state for passive reservoir. (b) EM stress versus length at steady state.

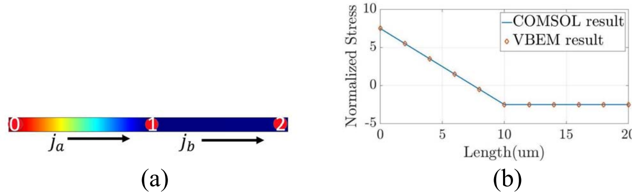

Fig. 9. (a) 2-D stress distribution on wire at steady state for passive sink. (b) EM stress versus length at steady state.

of the circuit and may not be the same. Then, the EM stress equation becomes

$$\begin{aligned} &V_0 = 0, \quad A_0 = l_a w_a, \quad \sigma_0 = \beta V_E \\ &V_1 = j_a l_a \rho, \quad A_1 = l_a w_a + l_b w_b, \quad \sigma_1 = \beta(V_E - V_1) \\ &V_2 = j_b l_b \rho + j_a l_a \rho, \quad A_2 = l_b w_b, \quad \sigma_2 = \beta(V_E - V_2) \\ &A = A_0 + A_1 + A_2 \end{aligned}$$

where

$$V_E = \frac{V_0 A_0 + V_1 A_1 + V_2 A_2}{2A} = \frac{V_1 A_1 + V_2 A_2}{2A}$$

where $\beta = (eZ/\Omega)$.

Passive sink and passive reservoir configurations, described in [24], are typical elements in the general interconnect tree. They are used as test cases in this section. Figs. 8 and 9 show the steady-state stress for the cases with passive reservoir (segment a with $j_a = 0$) and passive sink (segment b with $j_b = 0$). Here, we define "passive" and "active" as representing zero current density and nonzero current density, respectively. The analysis will focus on mitigating the EM effect in the active segment. It can be observed from Fig. 8 that the passive reservoir (segment a) is characterized with higher stress compared with the active sink (segment b). Thus, the void will first nucleate in the reservoir which can relax the EM effect in the sink. On the contrary, as shown in Fig. 9, the existence of passive sink (segment b) will lead to higher stress in the active reservoir (segment a), which accelerates the void formation thus leading to EM failure in the reservoir. A comparison of the steady-state stress predicted by VBEM with the FEA (COMSOL) simulation in both cases has demonstrated an excellent agreement.

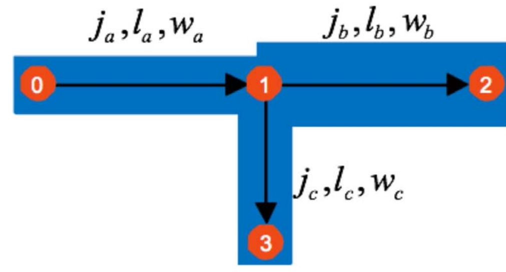

Fig. 10. Interconnect examples for EM analysis for T-shaped 4-terminal wire.

2) T-Shaped 4-Terminal Wire With Stub: The structure of the T-shaped 4-terminal wire is shown in Fig. 10. In this case, we have three segments which connect through the middle node 1. Current densities are j_a, j_b, and j_c on the three branches. In this case, if we make the branch c (the vertical branch), the stub (its current density is set to zero, $j_c = 0$), then the EM stress can also be obtained

$$\begin{aligned} &V_0 = 0, \quad A_0 = l_a w_a \\ &V_1 = j_a l_a \rho, \quad A_1 = l_a w_a + l_b w_b + l_c w_c \\ &V_2 = j_b l_b \rho + j_a l_a \rho, \quad A_2 = l_b w_b \\ &V_3 = j_a l_a \rho + j_c l_c \rho, \quad A_3 = l_c w_c \\ &\sigma_0 = \beta V_E, \quad \sigma_1 = \beta(V_E - V_1) \\ &\sigma_2 = \beta(V_E - V_2), \quad \sigma_3 = \beta(V_E - V_3) \\ &A = A_0 + A_1 + A_2 + A_3 \end{aligned}$$

where

$$V_E = \frac{V_1 A_1 + V_2 A_2 + V_3 A_3}{2A}.$$

The stub acts as a sink when it is close to an anode and serves as a source when it is close to a cathode. The distance between the stub and the cathode and the length of the stub can be important factors related to EM stress. As shown in Fig. 2(b), when the stub is moved away from the cathode node (node 0), it allows more atoms to migrate to the stub and thus creates more tensile stress at the cathode node. This is a commonly seen structure in interconnect circuit design. We will discuss the effects of the distance between the stub and the cathode as well as the length of the stub on EM stress. Thus, by adjusting the stub location and length, we can adjust the stress at the cathode node to fix potential EM failures in the physical design.

3) Interconnect Wires With Comb Structure: Now, we study a more complicated interconnect structure, which is the comb or ladder structure as shown in Fig. 11.

In this comb-structured interconnect, we have N fingers, in which each finger structure is assumed to be the same. R_{sh} is the sheet resistance of the metal and I is the current along each finger. We assume that node 0 is still the ground node. L_B and W_B are the length and width, respectively, for the body structures, L_F and W_F are the length and width, respectively, for the fingers. i refers to ith node on the body and i' is the node on the ith finger.

The total area connected to node k, except node N, is A_k and total area connected to node k' is $A_k{}'$, total area connected to

Authorized licensed use limited to: Univ of Calif Riverside. Downloaded on June 24,2026 at 00:38:02 UTC from IEEE Xplore. Restrictions apply.

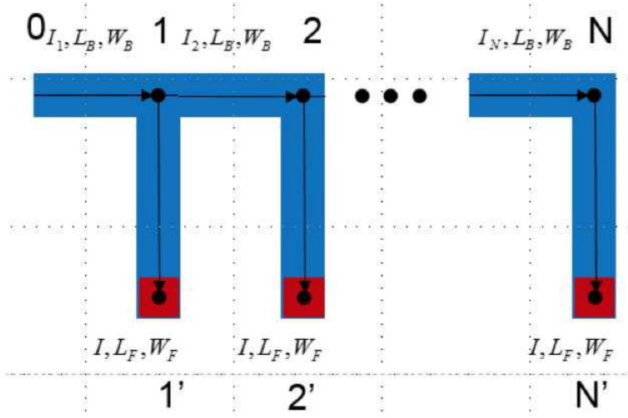

Fig. 11. Comb structure interconnect examples for EM analysis.

node N is A_N, and the total area of the whole comb structures, A, can be expressed as

$$\begin{aligned} A_k &= 2W_BL_B + W_FL_F, \quad A_k{}' = W_FL_F \\ A_N &= W_BL_B + W_FL_F \\ A &= N(W_BL_B + W_FL_F). \end{aligned}$$

Note that since the Nth node is only connected to one part of the body structure, the total area connected with node N is different from other nodes. Current flows in the same direction (which is opposite to the arrows in the figure), the highest EM tensile stress will be generated at node 0 because it has the lowest potential. Hence, in this case, we only need to check V_E against the critical potential.

The potential at each node for V_k and $V_k{}'$ can be obtained as

$$\begin{aligned} V_k &= \left[Nk - \frac{k(k-1)}{2}\right] \times I \times \frac{L_B}{W_B} R_{sh} \\ V_k{}' &= V_k + I \times \frac{L_F}{W_F} R_{sh}. \end{aligned}$$

Finally, the EM stress of the comb structure can be obtained as

$$\begin{aligned} V_E = \frac{IR_{sh}}{12} \times \Bigg[&\frac{(N+1)(4N-1){L_B}^2}{W_BL_B + W_FL_F} \\ &+ \frac{2(N+1)(2N+1)L_BL_FW_F/W_B + 6{L_F}^2}{W_BL_B + W_FL_F} \Bigg] \\ \sigma_0 = \beta V_E. & \end{aligned} \tag{34}$$

As shown in the above equation, three factors, N, L_F, and L_B have a strong influence on stress. Fig. 12 shows how the EM-induced stresses at the node 0 change with L_F and L_B. As we can see, L_B has a much larger impact on the stress than L_F, which can be used for EM optimization. Both L_F and L_B have nonlinear impacts on the stress and this nonlinear trend is more clear for L_F

Other trends of stress change will be analyzed and discussed in the numerical results section.

F. Current Crowding Impact Analysis

In this section, we study the impact of the current density distributions on the proposed VBEM analysis method.

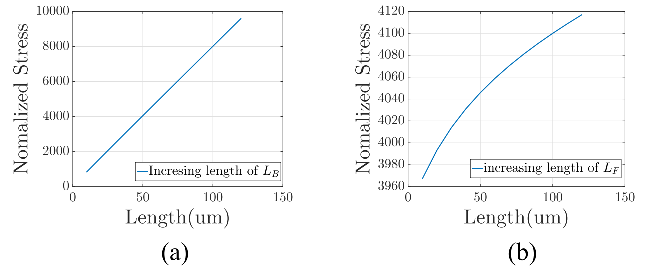

Fig. 12. (a) EM stress validation for each comb structure interconnect with changing L_B. (b) EM stress validation for each comb structure interconnect with changing L_F.

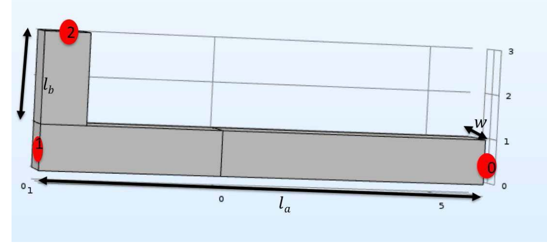

Fig. 13. L-shaped wire structure with three nodes.

The VBEM method assumes that current density is evenly distributed. However, this is not always the case since for real interconnect wires, the current density may vary and become larger around the corner areas (the current crowding effect). We observe that if the width is not much smaller than the segment length, the current crowding effect can be quite significant. In this case, the calculated nodal voltage will be less accurate for stress calculations.

To consider the current crowding effects, instead of using (12) to compute the *EM voltage*, we need to perform the area integration of voltage using (13) to compute the final steady-state stress after current and voltage distributions are computed. As we will show in this section, this will lead to more accurate results compared to the results using (12), and that the proposed method can be extended to consider current crowding effects. The area used for the integration is the total areas of the wires in 2-D case (although we show 3-D structures of the wires) since (13) is for 2-D integration. In principle, the integration can be done over the 3-D volume. It does not have to be restricted to 2-D integration. We also remark that the VBEM method will be more expensive for the numerical 2-D integration operation. This is due to the nature of the current crowding modeling problem. One has to compute the detailed current and voltage distributions first using expensive numerical methods such as the finite element method, to account for the effects of current crowding on EM risks.

In the following, we study two wire structures to assess the impact of current crowding effects. In Fig. 13, an L-shaped wire with three nodes is used as the first test structure. Here, l_a and l_b are not much larger than the width of wire w. A voltage is applied on nodes 1 and 0 is the ground node. Node 2 is connected with node 1 through a stub with a current density of 0.

Authorized licensed use limited to: Univ of Calif Riverside. Downloaded on June 24,2026 at 00:38:02 UTC from IEEE Xplore. Restrictions apply.

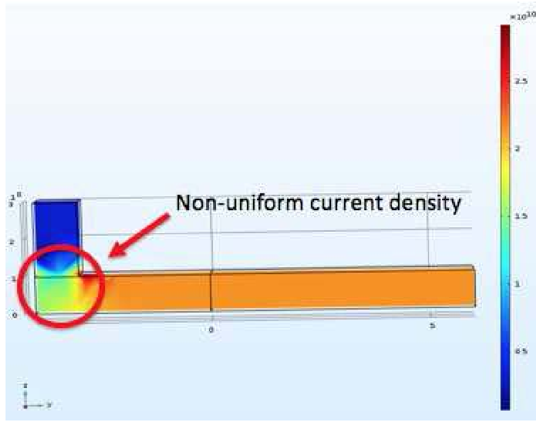

Fig. 14. L-shaped wire structure with current-crowding effects.

TABLE II
EM STRESS CALCULATED WITH AND WITHOUT CURRENT-CROWDING EFFECTS

Cases	COMSOL	Crowding	Err1	NoCrowding	Err2
1	286MPa	284MPa	0.94%	282MPa	1.53%
2	97.7MPa	96.1MPa	1.60%	90.4MPa	7.72%

TABLE III
STRESS VALUES AT EACH NODE FOR THE U-SHAPED STRUCTURE

Cases/Nodes	1	2	3	4
COMSOL	345.5Mpa	104.2Mpa	-104.2Mpa	-345.5Mpa
Crowding	339.0MPa	102.2MPa	-102.2MPa	-339.0Mpa
Error	1.74%	1.95%	1.95%	1.74%
No Crowding	339Mpa	135.6Mpa	-135.6Mpa	-339Mpa
Error	1.74%	23.16%	23.16%	1.74%

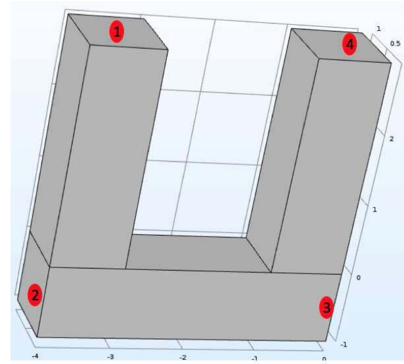

Fig. 15. U-shaped wire structure with four nodes.

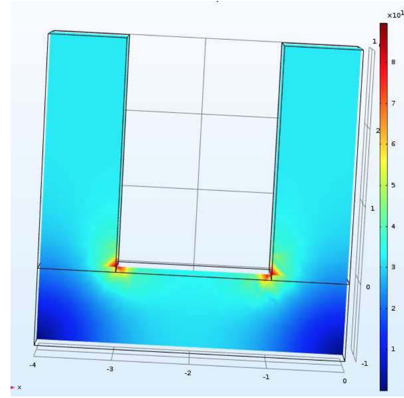

Fig. 16. U-shaped wire structure with current-crowding effects.

In this case, the current density distribution around node 1 is not uniform, as shown in Fig. 14. COMSOL simulation is used to obtain that nonuniform current density distribution as well as voltage distribution. At node 1, the current density is smaller than the current density on the other part of the branch. This means that if the nodal voltage is used to calculate the stress, it will be smaller than the actual condition. On the other hand, if the branch is longer (compared to the width of the wire), the current crowding has a smaller effect on the final steady-state stress.

Table II summarizes the results for two cases for the stress values at the cathode node. In case 1, $l_a = 10$, $l_b = 2$, and $j = 3$ MA/cm^2 with voltage difference 0.03 V between nodes 0 and 1, In case 2, $l_a = 4$, $l_b = 2$, and $j = 3$ MA/cm^2 with voltage difference is 0.012 V between nodes 0 and 1. Column *crowding* indicates that the current-crowding effect is considered by using (13) and *Err1* is the relative error of considering the crowding effect compared to COMSOL. Column *noCrowding* indicates that no current crowding effect is computed using (12) and *Err2* is the error without considering the crowding effect.

As we can see from Table II, for the long branch (case 1), the error for the method without considering current crowding is 1.53% and the error increases to 7.72% for the shorter branch (case 2), which is quite significant. However, if the current crowding effect is considered (as shown in *Crowding* column), the errors become smaller (less than 2%).

The second structure we study is the U-shaped wire shown in Fig. 15. Its segment length is not significantly larger than the width in this case and current density distribution can be seen in Fig. 16, with the current-crowding effect being very visible at nodes 2 and 3.

For the U-shaped structure, we apply 0.05 V to node 1 and 0 V voltage to node 4. The result is shown in Table III for the stress values at the four nodes. Row *Crowding* indicates that the current-crowding effect is considered and row *noCrowding* indicates that the crowding effect is not considered.

As we can see, for nodes 1 and 4, even when current crowding is not considered, the error is only 1.74%, which is close to the errors of cases considering current crowding. However, for nodes 2 and 3 if current crowding is not considered, the errors increase to 23.16%. On the other hand, the error reduces to 1.95% when current crowding is considered. Thus, in both cases, if the wire segment is long enough (more than ten times of wire width), the current-crowding impact on stress values by the VBEM method is not significant.

G. Application to Mesh-Structured Interconnect Wires

In this section, we study if the proposed VBEM analysis method can be applied to mesh-structured interconnect wires, which can be used at the cell-level layout design and can be vulnerable to EM failure as well.

Fig. 17 shows a 4 × 4 mesh structure with 16 nodes. In order to calculate the V_E, nodal voltages and areas connected

Authorized licensed use limited to: Univ of Calif Riverside. Downloaded on June 24,2026 at 00:38:02 UTC from IEEE Xplore. Restrictions apply.

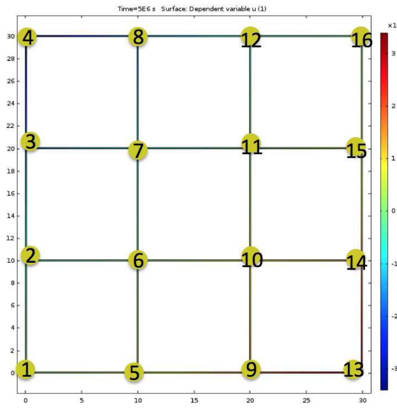

Fig. 17. 4 × 4 mesh-structured wire.

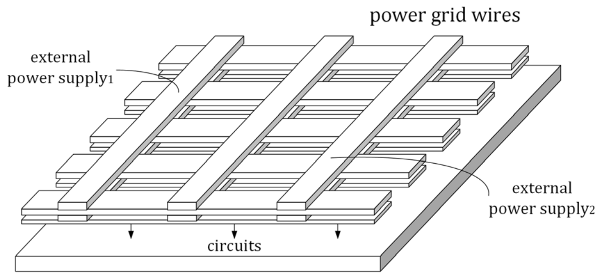

Fig. 18. Small portion of a typical power supply network [25].

TABLE IV
STRESS CONDITION FOR MESH STRUCTURE

Nodes	1	2	3	4
Voltage	2.498e-3V	2.880e-3V	3.656e-3V	5e-3V
COMSOL	0.2441Mpa	-51.61MPa	-157.0Mpa	-339.5MPa
VBEM	0.2439Mpa	-51.53Mpa	-156.8Mpa	52.07Mpa
Error	0.0771%	0.1549%	0.1572%	0.1609%
Nodes	5	6	7	8
Voltage	2.116e-3V	2.498e-3V	3.079e-3V	3.652e-3V
COMSOL	52.15Mpa	0.2118MPa	-78.62Mpa	-156.6MPa
VBEM	52.07Mpa	0.2116Mpa	-78.50Mpa	-156.3Mpa
Error	0.1543%	0.095%	0.1547%	0.1572%
Nodes	9	10	11	12
Voltage	1.347e-3V	1.921e-3V	2.502e-3V	2.884e-3V
COMSOL	156.8Mpa	78.62MPa	-0.2114Mpa	-52.15MPa
VBEM	156.3Mpa	78.50Mpa	-2.110Mpa	-52.07Mpa
Error	0.1571%	0.1545%	0.1529%	0.1545%
Nodes	13	14	15	16
Voltage	0	1.344e-3V	2.120e-3V	0.250e-3V
COMSOL	338.5Mpa	157.0MPa	51.61Mpa	-0.2441MPa
VBEM	339.8Mpa	156.8Mpa	51.53Mpa	-0.2438Mpa
Error	0.1543%	0.095%	0.1547%	0.1572%

TABLE V
PROPERTY OF IBM BENCHMARKS

Name	ibmpg1	ibmpg2	ibmpg3	ibmpg4
#node	11572	61797	407279	474836
#branch	5580	61143	399201	384709
#max branch	30	192	965	571
#trees	689	462	7388	9358
#failed trees	249	91	1585	0
VBEM(s)	0.69	29.63	3999.97	4565.27
Baseline(s)	910.56	973.65	17720.97	22456.13
Acceleration	1319X	30.86X	4.43X	4.91X

with each node are required. A voltage is applied on nodes 4 and 13 is set to be ground node. The voltage of each node can be measured or analyzed by SPICE. Areas connected to each node are different at different locations. For the nodes at corners (1,4,13,16), the area connected with them is $2WL$, where W is the width of the wire and L is the distance between adjacent nodes.

For the nodes at the boundaries (2,3,5,8,9,12,14,15), the area connected with them is $3WL$. For the nodes in the middle (6,7,10,11), the area connected with them is $4WL$. The total area is the area summation of each branch, which is $48WL$. Then the V_E can be obtained as

$$\begin{aligned} V_E = &\ (2WL(V_1 + V_4 + V_13 + V_16) \\ &+ 3WL(V_2 + V_3 + V_5 + V_8 + V_9 + V_12 \\ &+ V_14 + V_15) \\ &+ 4WL(V_6 + V_7 + V_10 + V_11))/48WL \\ \sigma_{\max} = &\ \sigma_{13} = \beta V_E. \end{aligned}$$

In our stressing set up, we apply 0.005 V to node 4 and 0 V (ground) to node 13. The length of each branch is 10 um and width is 0.1 um. Table IV shows the result of the test case. As we can see, for all the cases, the VBEM method leads to less than 0.17% error compared to COMSOL, which shows that the proposed VBEM method can be directly applied to mesh-structured wires.

H. Application to IBM Power Grids

Besides small interconnect structures, we also validate the proposed method on a large practical IBM power grid benchmark [25]. A portion of the power grid network is shown in Fig. 18. Details of the benchmark are shown in Table V. In this experiment, critical stress is 500 MPa [26]. The critical voltage is 3.694×10^{-3} V. For the IBM power grid networks, COMSOL based FEM analysis method is too slow. Instead, we use a recently proposed eigen-function-based stress analysis method for multisegment interconnect trees [14] as the baseline for comparison. The proposed VBEM and baseline methods were both implemented with C/C++ for comparison. The comparison works were carried out on a workstation with 2 Intel Xeon E5-2698 CPUs and 128 GB memory.

We can see thatthe VBEM method has significant acceleration compared to the baseline method. For *ibmpg1*, VBEM takes only 0.69 s to simulate all 689 trees, which translates to a 1319X speed-up over the baseline method. All the trees in *ibmpg1* are small trees with the maximum number of branches in a tree being 30. With larger trees, the acceleration rate decreases, but one still sees 30.86× acceleration for *ibmpg2*, 4.43× acceleration for *ibmpg3*, and 4.91× acceleration for *ibmpg4*. Note that the lengths of branches are not the same. As can be seen in *ibmpg4*, although it has trees with many branches, the lengths of branches are small so all trees are immortal in this case.

We note that the baseline method is a transient EM analysis while the VBEM method is a steady-state method. Another saving brought by the VBEM method is the percentage of the immortal tree count over the total tree count, as the immortal trees will not need the costly transient EM analysis. The immortal tree number can be significant compared to the total tree count (ranging from 63.8% in *ibmpg1* to 100% in *ibmpg4*

Authorized licensed use limited to: Univ of Calif Riverside. Downloaded on June 24,2026 at 00:38:02 UTC from IEEE Xplore. Restrictions apply.

TABLE VI
PARAMETERS FOR EACH STRAIGHT-LINE 3-TERMINAL INTERCONNECT CASE

Case	Branch a			Branch b		
	l	w	j	l	w	j
	μm	μm	MA/cm^2	μm	μm	MA/cm^2
1	25	1	1.25	0	1	0
2	25	1	1.25	175	1	0
3	25	1	1.25	175	1	0.125
4	25	1	1.25	175	1	0.625
5	25	1	1.25	175	1	1.25
6	10	0.1	10	25	1.25	1.25
7	10	0.2	5	25	1.25	1.25
8	10	0.3	3.3	25	1.25	1.25
9	10	0.4	2.5	25	1.25	1.25
10	10	0.5	2	25	1.25	1.25

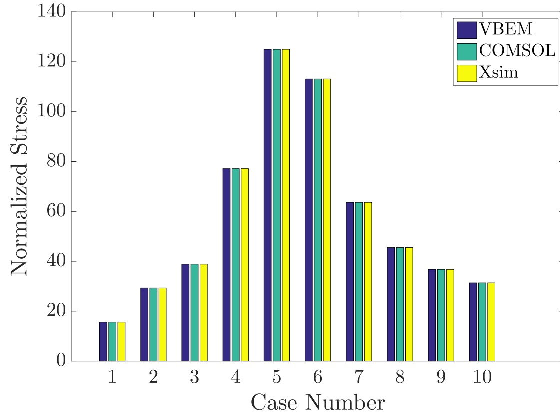

Fig. 19. Steady-state EM stress comparisons for each straight-line 3-terminal interconnect case [x: case number, y: EM stress at the node 0 (cathode node)].

TABLE VII
PARAMETERS FOR EACH T-SHAPED 4-TERMINAL INTERCONNECT CASE ($l = \mu$m, $w = \mu$m, AND $j =$ MA/cm^2)

Branch	Case	1	2	3	4	5	6
a	l	6	10	11	20	20	20
	w	0.14	0.14	0.14	0.14	0.28	0.28
	j	7.142	7.142	7.142	7.142	3.571	3.571
b	l	4	0	9	0	0	0
	w	0.14	0.14	0.14	0.14	0.28	0.28
	j	7.142	7.142	7.142	7.142	3.571	3.571
c	l	5	5	10	10	5	10
	w	0.28	0.28	0.14	0.14	0.14	0.14
	j	0	0	0	0	0	0

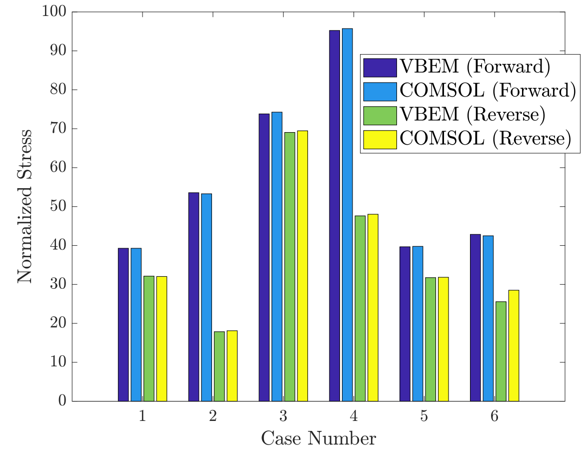

Fig. 20. EM stress validations for each T-shaped 4-terminal interconnect case [x: case number, y: EM stress at the node 0 (cathode node)].

case. Hence, the percentage of savings from the proposed VBEM method is problem-specific and can be very significant.

IV. NUMERICAL VALIDATION RESULTS AND DISCUSSION

In this section, we validate the proposed VBEM check tool against numerical analysis results. We validate the VBEM method against the results by an FEA tool, COMSOL [27], based on the dynamic stress evolution described by Korhonen's equation (6). In the following, we list the results for the three structures we have discussed.

A. Results for Straight-Line 3-Terminal Interconnects

The parameters used for the validation cases are summarized in Table VI and the results for the 3-terminal wire are shown in Fig. 19, which shows the largest tensile stress at node 0. We compare our results against COMSOL and another published EM numerical simulator, XSim [19], which has been validated by measured results [19], [20].

As demonstrated in Fig. 19, the results of the proposed method agree well with COMSOL results. To further validate the new method, we compared our results against the EM simulator XSim for steady-state results. As we can see, the VBEM method also agrees very well with XSim, which further validates the proposed method. With the increase in length and current density in the branch b, the EM stress increases. If the current density in branch a decreases, EM stress also decreases.

B. Results for T-Shaped 4-Terminal Interconnect

We next validate the VBEM method on the T-shaped 4-terminal interconnect case. Again, we list the parameters used for the validation cases in Table VII and results of 3-terminal wires are shown in Fig. 20, which shows the largest tensile stress at the node 0.

During the analysis of the T-shaped interconnect, forward and reverse currents are provided in branches a and b. Again, we observe that the obtained results are also very close to COMSOL results and the average error rate is 0.56% while the maximum error is 1.42% in case 2 reverse. Also, it can be seen if the total length of branches a and b increases, the stress increases. Furthermore, the location and current density of the stub can have a significant impact on the stress at the stub (branch c). With zero current density, the stub can decrease the stress if it is closer to the cathode, or if its length is decreased. Also, if the stub is placed further away from the cathode and its length is longer, the stress increases.

C. Results for Comb Structure Interconnects

Now, we further validate the proposed VBEM method on the comb-structured interconnect. We list the parameters used for different test cases and the predicted stress and error rate in Table VIII. Fig. 21 shows the impact of the number of fingers, N, on the stress at the node 0 for these three cases or configurations. As we can see, with an increase in N, the EM stress increases super-linearly. Besides, we can observe from Fig. 12 that, increasing L_B and L_F increases EM-induced stress at node 0. However, the increase in L_F only has a small effect on

Authorized licensed use limited to: Univ of Calif Riverside. Downloaded on June 24,2026 at 00:38:02 UTC from IEEE Xplore. Restrictions apply.

TABLE VIII
EM STRESS VALIDATIONS FOR COMB STRUCTURE INTERCONNECT CASES

Comb Case	Method	Number of fingers					
		1	2	4	6	8	10
Case 1 - $W_B = 1, W_F = 1$, $L_B = 10, L_F = 10$	**Proposed EM**	10	23.75	71.25	145.42	246.25	373.75
	COMSOL	10	23.78	71.33	146.50	245.10	375.88
	Error	0.00%	0.08%	0.11%	0.74%	0.47%	0.57%
Case 2 - $W_B = 1, W_F = 1$, $L_B = 20, L_F = 10$	**Proposed EM**	15	41.67	135	281.67	481.67	735
	COMSOL	15	41.59	136.28	279.80	486.41	738.12
	Error	0.00%	0.18%	0.94%	0.67%	0.98%	0.42%
Case 3 - $W_B = 1, W_F = 1$, $L_B = 10, L_F = 20$	**Proposed EM**	15	29.17	77.5	152.5	254.17	382.5
	COMSOL	15	29.42	77.19	152.07	257.51	385.73
	Error	0.00%	0.85%	0.41%	0.28%	1.30%	0.84%

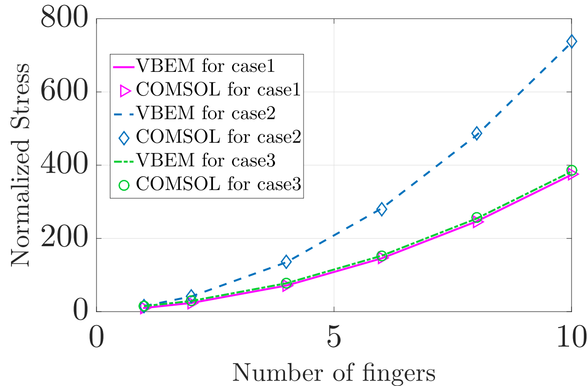

Fig. 21. EM stress validations for each comb structure interconnect case [*x*: number of fingers, *y*: EM stress at the node 0 (cathode node)]

EM stress as compared to the increase in L_B. Furthermore, the results of the VBEM approach show good agreement with the results obtained from COMSOL. The average error is 0.49% and maximum error is 1.3% in case 3 at $N = 8$.

V. CONCLUSION

As VLSI technology features are pushed to the limit with every generation and with the introduction of new materials and increased current densities to satisfy performance demands, the risk of EM failure is ever-increasing. In this paper, we have presented a novel and fast EM immortality check for general multibranch interconnect trees. The new method estimates the EM-induced steady-state stress in general multisegment copper interconnect wires based on a novel parameter, $V_{\text{Crit,EM}}$. We have shown that the $V_{\text{Crit,EM}}$ essentially is the natural, but important extension of the *Blech product* or *Blech limit* concept, which describes the EM immortality condition for a single-segment wire, to more general multisegment interconnect wires. Furthermore, the new VBEM analysis method is very amenable for EM violation fixing as it brings new design knobs and capabilities into the physical design flow. The resulting EM risk assessment method can be much easier to integrate with physical design tools and flows. The new VBEM stress estimation method is based on the exact solution of fundamental steady-state stress equations. We have shown that the proposed VBEM analysis method agrees with the results from the finite difference method in the steady-state through one example and also agrees with one published closed-form expression of steady-state stress for a special 3-terminal wire case, which further validates the proposed method. Furthermore, we compared VBEM against the COMSOL FEA tool and another published EM numerical simulator XSim and it was shown that the VBEM approach agrees with both of them very well in terms of accuracy. We also studied the impact of the current crowding of practical interconnect wires on the estimated steady-state stress and showed that the effect is not significant if the length of the wire length is much greater than its width. An extension of the VBEM method to consider the significant current crowding effects was given and additionally, we analyzed mesh-structured interconnect wires and demonstrated that the proposed VBEM method is correct and accurate on these structures as well.

ACKNOWLEDGMENT

The authors would like to thank Prof. C. V. Thompson of MIT and Prof. G. C. Lip of Nanyang Technological University for sharing the electromigration simulator—XSim, which was used in this paper for comparison.

REFERENCES

[1] J. R. Black, "Electromigration—A brief survey and some recent results," *IEEE Trans. Electron Devices*, vol. ED-16, no. 4, pp. 338–347, Apr. 1969.
[2] I. A. Blech, "Electromigration in thin aluminum films on titanium nitride," *J. Appl. Phys.*, vol. 47, no. 4, pp. 1203–1208, 1976.
[3] B. Bailey, "Thermally challenged," in *Semiconductor Engineering*. San Jose, CA, USA: Sperling Media Group LLC, 2013.
[4] C. V. Thompson, S. P. Hau-Riege, and V. K. Andleigh, "Modeling and experimental characterization of electromigration in interconnect trees," in *Proc. AIP Conf.*, vol. 491, 1999, pp. 62–73.
[5] S. Hau-Riege, "New methodologies for interconnect reliability assessments of integrated circuits," Ph.D. dissertation, Dept. Mater. Sci. Eng., Massachusetts Inst. Technol., Cambridge, MA, USA, Jun. 2000.
[6] A. Abbasinasab and M. Marek-Sadowska, "Blech effect in interconnects: Applications and design guidelines," in *Proc. Symp. Int. Symp. Phys. Design (ISPD)*, Monterey, CA, USA, 2015, pp. 111–118.
[7] J. S. Pak, M. Pathak, S. K. Lim, and D. Z. Pan, "Modeling of electromigration in through-silicon-via based 3D IC," in *Proc. IEEE 61st Electron. Compon. Technol. Conf. (ECTC)*, 2011, pp. 1420–1427.
[8] M. Pathak, J. S. Pak, D. Z. Pan, and S. K. Lim, "Electromigration modeling and full-chip reliability analysis for BEOL interconnect in TSV-based 3D ICs," in *Proc. IEEE/ACM Int. Conf. Comput.-Aided Design (ICCAD)*, San Jose, CA, USA, 2011, pp. 555–562.
[9] X. Zhao, Y. Wan, M. Scheuermann, and S. K. Lim, "Transient modeling of TSV-wire electromigration and lifetime analysis of power distribution network for 3D ICs," in *Proc. IEEE/ACM Int. Conf. Comput.-Aided Design (ICCAD)*, San Jose, CA, USA, 2013, pp. 363–370.
[10] J. Pak, S. K. Lim, and D. Z. Pan, "Electromigration study for multiscale power/ground vias in TSV-based 3D ICs," in *Proc. IEEE/ACM Int. Conf. Comput.-Aided Design (ICCAD)*, San Jose, CA, USA, 2013, pp. 379–386.

Authorized licensed use limited to: Univ of Calif Riverside. Downloaded on June 24,2026 at 00:38:02 UTC from IEEE Xplore. Restrictions apply.

[11] X. Huang, Y. Tan, V. Sukharev, and S. X.-D. Tan, "Physics-based electromigration assessment for power grid networks," in *Proc. Design Autom. Conf. (DAC)*, San Francisco, CA, USA, Jun. 2014, pp. 1–6.
[12] M. A. Korhonen, P. Bo/rgesen, K. N. Tu, and C.-Y. Li, "Stress evolution due to electromigration in confined metal lines," *J. Appl. Phys.*, vol. 73, no. 8, pp. 3790–3799, 1993.
[13] H.-B. Chen, S. X.-D. Tan, V. Sukharev, X. Huang, and T. Kim, "Interconnect reliability modeling and analysis for multi-branch interconnect trees," in *Proc. Design Autom. Conf. (DAC)*, San Francisco, CA, USA, Jun. 2015, pp. 1–6.
[14] X. Wang *et al.*, "Physics-based electromigration modeling and assessment for multi-segment interconnects in power grid networks," in *Proc. Design Autom. Test Europe. (DATE)*, Lausanne, Switzerland, Mar. 2017, pp. 1727–1732.
[15] C. Cook, Z. Sun, T. Kim, and S. X.-D. Tan, "Finite difference method for electromigration analysis of multi-branch interconnects," in *Proc. Int. Conf. Synth. Model. Anal. Simulat. Methods Appl. Circuit Design (SMACD)*, Lisbon, Portugal, 2016, pp. 1–4.
[16] S. Chatterjee, V. Sukharev, and F. N. Najm, "Power grid electromigration checking using physics-based models," *IEEE Trans. Comput.-Aided Design Integr. Circuits Syst.*, to be published.
[17] E. Demircan and M. D. Shroff, "Model based method for electromigration stress determination in interconnects," in *Proc. IEEE Int. Rel. Phys. Symp.*, Jun. 2014, pp. IT.5.1–IT.5.6.
[18] Z. Sun *et al.*, "Voltage-based electromigration immortality check for general multi-branch interconnects," in *Proc. Int. Conf. Comput. Aided Design (ICCAD)*, Austin, TX, USA, Nov. 2016, pp. 1–7.
[19] F. L. Wei *et al.*, "Electromigration-induced extrusion failures in Cu/low-k interconnects," *J. Appl. Phys.*, vol. 104, no. 2, pp. 1–10, 2008.
[20] C. S. Hau-Riege, A. P. Marathe, and Z.-S. Choi, "The effect of current direction on the electromigration in short-lines with reservoirs," in *Proc. IEEE Int. Rel. Phys. Symp. (IRPS)*, Phoenix, AZ, USA, 2008, pp. 381–384.
[21] V. Sukharev, "Beyond black's equation: Full-chip EM/SM assessment in 3D IC stack," *Microelectron. Eng.*, vol. 120, pp. 99–105, May 2014.
[22] V. Sukharev, "Physically based simulation of electromigration-induced degradation mechanisms in dual-inlaid copper interconnects," *IEEE Trans. Comput.-Aided Design Integr. Circuits Syst.*, vol. 24, no. 9, pp. 1326–1335, Sep. 2005.
[23] A. Kteyan, V. Sukharev, M.-A. Meyer, E. Zschech, and W. D. Nix, "Microstructure effect on EM-induced degradations in dual-inlaid copper interconnects," *AIP Conf. Proc.*, vol. 945, no. 1, pp. 42–55, 2007.
[24] M. H. Lin and A. S. Oates, "An electromigration failure distribution model for short-length conductors incorporating passive sinks/reservoirs," *IEEE Trans. Device Mater. Rel.*, vol. 13, no. 1, pp. 322–326, Mar. 2013.
[25] S. R. Nassif, "Power grid analysis benchmarks," in *Proc. Asia South Pac. Design Autom. Conf. (ASPDAC)*, Seoul, South Korea, 2008, pp. 376–381.
[26] R. Gleixner and W. D. Nix, "A physically based model of electromigration and stress-induced void formation in microelectronic interconnects," *J. Appl. Phys.*, vol. 86, no. 4, pp. 1932–1944, 1999.
[27] *COMSOL Multiphysics*. Accessed: Oct. 16, 2013. [Online]. Available: https://www.comsol.com/

Zeyu Sun (S'16) received the B.S. degree in electronic and computer engineering from the Hong Kong University of Science and Technology, Hong Kong, in 2015. He is currently pursuing the Ph.D. degree with the Department of Electrical and Computer Engineering, University of California at Riverside, Riverside, CA, USA.

His current research interests include electromigration modeling and assessment and reliability-aware performance optimization.

Ertugrul Demircan (M'97–SM'02) received the B.S. degrees in EE and physics from Boğaziçi University, Istanbul, Turkey and the Ph.D. degree in physics from the University of Texas at Austin, Austin, TX, USA.

He is a member of the PDK Team, NXP Semiconductors, Inc., Austin. TX, USA. Since 1995, he has been researching on a wide range of technologies from 0.25 um to 7 nm on interconnect modeling and parasitic extraction, interconnect reliability, and development of novel physical verification methodologies. He has several conference and journal publications and eight issued patents.

Mehul D. Shroff received the B.Tech. degree in chemical engineering from the Indian Institute of Technology Bombay, Mumbai, India, in 1993, the M.S. degree in chemical engineering from the University of New Mexico, Albuquerque, NM, USA, in 1995, and the M.S. degree in software engineering from the University of Texas, Austin, TX, USA, in 2002.

He manages the Global Intrinsic Reliability Team, NXP Semiconductors, Inc., Austin, TX, USA. He has researched in various engineering and technical management roles in the semiconductor industry since 1995 across multiple generations of submicron technologies.

Chase Cook (S'14) received the B.S. degree in computer engineering from California State University, Bakersfield, CA, USA, in 2015. He is currently the Ph.D. degree with the Department of Electrical and Computer Engineering, University of California at Riverside, Riverside, CA, USA.

His current research interests include electronic design automation and simulation of aging effects in integrated circuits.

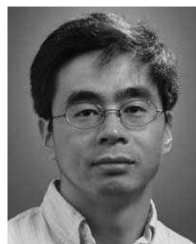

Sheldon X.-D. Tan (S'96–M'99–SM'06) received the B.S. and M.S. degrees in electrical engineering from Fudan University, Shanghai, China, in 1992 and 1995, respectively, and the Ph.D. degree in electrical and computer engineering from the University of Iowa, Iowa City, IA, USA, in 1999.

He is a Professor with the Department of Electrical Engineering, University of California at Riverside, Riverside, CA, USA, where he also is a Cooperative Faculty Member with the Department of Computer Science and Engineering and is the Associate Director of Computer Engineering Program. He was a Visiting Professor with Kyoto University, Kyoto, Japan, as a JSPS Fellow, in 2017. His current research interests include VLSI reliability modeling, optimization and management at circuit and system levels, thermal modeling, optimization and dynamic thermal management for many-core processors, statistical modeling, simulation and optimization of mixed-signal/RF/analog circuits, parallel circuit simulation techniques based on GPU and multicore systems.

Dr. Tan was a recipient of the Outstanding Oversea Investigator Award from the National Natural Science Foundation of China in 2008, the NSF CAREER Award in 2004, the Best Paper Award from 2007 IEEE International Conference on Computer Design (ICCD'07), the Best Paper Award from 1999 IEEE/ACM Design Automation Conference, three Best Paper Award Nomination from the IEEE/ACM Design Automation Conferences in 2005, 2009, and 2014, and one Best Paper Award Nomination from ASP-DAC in 2015. He is serving as the Editor-in-Chief for *Integration, The VLSI Journal*. He is also serving as an Associate Editor for three journals including the IEEE TRANSACTION ON VERY LARGE SCALE INTEGRATION SYSTEMS, *ACM Transaction on Design Automation of Electronic Systems*, and *Microelectronics Reliability*.

Authorized licensed use limited to: Univ of Calif Riverside. Downloaded on June 24,2026 at 00:38:02 UTC from IEEE Xplore. Restrictions apply.